Neoplasia • Vol. 4, No. 6, 2002, pp. 480–485

www.nature.com/neo

MRI of Mouse Models for Gliomas Shows Similarities to Humans and Can Be Used to Identify Mice for Preclinical Trials

Jason A. Koutcher[*,†,‡], *Xiaoyi Hu*[§], *Su Xu**, *Terence P. F. Gade**, *Norman Leeds*[¶], *Xiaohong Joe Zhou*[¶], *David Zagzag*[#,**] *and Eric C. Holland*[††]

Departments of *Medical Physics, [†]Medicine, [‡]Radiology, [§]Cell Biology, Memorial Sloan Kettering Cancer Center, 1275 York Avenue, New York, NY 10021, USA; [¶]Department of Diagnostic Radiology, MD Anderson Cancer Center, 1515 Holcombe Boulevard, Houston, TX 77030, USA; Departments of [#]Pathology and **Neurosurgery, New York University School of Medicine, 550 First Avenue, New York, NY 10016, USA; [††]Department of Surgery (Neurosurgery) and Neurology, Memorial Sloan Kettering Cancer Center, 1275 York Avenue, New York, NY 10021, USA

Abstract

Magnetic resonance imaging (MRI) has been utilized for screening and detecting brain tumors in mice based upon their imaging characteristics appearance and their pattern of enhancement. Imaging of these tumors reveals many similarities to those observed in humans with identical pathology. Specifically, high-grade murine gliomas have histologic characteristics of glioblastoma multiforme (GBM) with contrast enhancement after intravenous administration of gadolinium diethylenetriamine pentaacetic acid (Gd-DTPA), implying disruption of the blood–brain barrier in these tumors. In contrast, low-grade murine oligodendrogliomas do not reveal contrast enhancement, similar to human tumors. MRI can be used to identify mice with brain neoplasms as inclusion criteria in preclinical trials.

Neoplasia (2002) **4,** 480–485 doi:10.1038/sj.neo.7900269

Keywords: MRI, brain tumor, screening, glioblastoma, oligodendrogliomas.

Introduction

The use of mouse models for human cancer in preclinical trials requires the identification of mice with tumors and quantitation of their tumor size for stratification, measurements of growth rate, and treatment response. In the case of mouse models for brain tumors, the identification of mice with tumors is complicated because of the inability to detect their presence because of their location within the cranial cavity. The development of noninvasive imaging techniques is necessary for maximizing the information available from these novel models.

In humans, low-grade gliomas are typically seen as areas of hypointense signal on T1 (spin–lattice relaxation time)–weighted scans and hyperintense signal on T2 (spin–spin relaxation time)–weighted scans, and do not enhance with gadolinium diethylenetriamine pentaacetic acid (Gd-DTPA) [1–3]. The biological properties that correlate with these imaging characteristics are proposed to be an intact blood–brain barrier and edema surrounding the tumor cells. In contrast, glioblastomas reveal marked contrast enhancement indicating a disrupted blood–brain barrier, and nonenhancing regions within the tumor that correlate with foci of necrosis [1–3]. Therefore, magnetic resonance imaging (MRI) is used to identify the presence of these tumors, to follow their response to therapy, and to provide evidence of residual or recurrence of disease.

MRI has been used to examine experimental brain tumors in rodents in diverse models [4–10]. Many of these studies utilized T1- and T2-weighted imaging techniques [4–6,8], which were found to be quantitative based upon phantom studies [6]. More recently, diffusion-weighted imaging has been added in brain tumor studies [9,10]. Chenevert et al. [5,9] suggested that diffusion-weighted imaging could provide a surrogate marker for treatment response in patients based upon rodent tumor studies. MRI and magnetic resonance spectroscopy (MRS) have also been used to study other tumor models and to provide metabolic and anatomic information [11–15]. Other imaging modalities including optical imaging [16–20], computed tomography [21], and radionuclide imaging have also been used to study rodent tumors [22–25].

MRI can be utilized to screen and identify mice harboring brain tumors, and the imaging characteristics of the tumors could potentially be used as one criterion of efficacy for strategies being developed and tested. In order to use such technology in this manner, baseline investigations correlating the imaging properties of brain tumors in mice with their histologic properties are necessary. Subsequent studies to determine how the tumor and its physiological parameters

Abbreviations: MRI, magnetic resonance imaging; T1, spin–lattice relaxation time; T2, spin–spin relaxation time; Gd-DTPA, gadolinium diethylenetriamine pentaacetic acid; PDGF, platelet-derived growth factor; TR, repetition interval; TE, echo time; FSE, fast spin echo; FOV, field of view

Address all correspondence to: Dr. Jason A. Koutcher, Department of Medical Physics, Memorial Sloan Kettering Cancer Center, 1275 York Avenue, New York, NY 10021, USA. E-mail: koutchej@mskcc.org

Received 30 May 2002; Accepted 10 July 2002.

Copyright © 2002 Nature Publishing Group All rights reserved 1522-8002/02/$25.00

have changed in response to treatment need to be done noninvasively. In order to perform such studies, mouse modeling systems that generate tumors with defined histologies mimicking human gliomas are required.

The RCAS/tv-a system has been used to generate several glioma types that are similar both in histology and genetics to that found in humans. This system utilizes avian RCAS retroviral vectors that transfer genes to mammalian cells only if they express the receptor for RCAS known as TVA [26]. TVA is not normally expressed in mammals but can be expressed as a transgene from tissue-specific promoters in transgenic mice. Two transgenic mouse lines that express tv-a from the nestin promoter (Ntv-a) [27] and the GFAP promoter (Gtv-a) [28] to support gene transfer into glial progenitors and astrocytes, respectively, have been used.

Oligodendrogliomas in this model are generated by transfer of platelet-derived growth factor (PDGF) to glial progenitors, generating an autocrine loop [29]. These PDGF-induced gliomas are predominantly low grade and show all the histological characteristics of oligodendrogliomas in humans including the classic "chicken wire vasculature" and invasion of adjacent normal brain structures. In contrast, the simultaneous activation of Ras and Akt signaling pathways in these same glial progenitors leads to the formation of tumors with histologic appearance of glioblastoma multiforme (GBM) [30]. These tumors reveal regions of nuclear pleomorphism, pseudopalisading necrosis, and microvascular proliferation.

The object of this study is to demonstrate that the MRI characteristics of the low- and high-grade gliomas in mice are similar to the equivalent human gliomas. Furthermore, the ability of MRI to identify mice with large gliomas for inclusion in preclinical trials is demonstrated.

Methods

The generation of the Ntv-a and Gtv-a mice has been described [27,28]. Ntv-a mice were infected at birth with RCAS vectors by intracranial injection of 1 μl of 10^4 DF-1 cells infected with and producing RCAS retroviral vectors, which has been previously described [27]. The mice were then observed for signs of intracranial pathology such as macrocephaly or lethargy. Such mice were anesthesized by the use of isoflurane and placed in the single mouse coil.

Single Mouse Imaging

Images were obtained on a 1.5-T General Electric LX Echo Speed Signa scanner (General Electric Medical Systems, Milwaukee, WI). Single animal images were obtained using a 2.9-cm-inner-diameter (7 cm in length), low-pass bird cage coil operating in quadrature and tuned to 63.9 MHz, specifically designed for mice studies (courtesy of Dr. Boskamp; General Electric Medical Systems). This coil was interfaced with the head coil port on the Signa system with an additional attenuation of 36 dB at the transmitter output. T1-weighted images {TR (repetition interval)=450 ms, TE (echo time)=9 ms} and T2-weighted images {FSE (fast spin echo), TR=4 s, TE=85 ms, and echo train length (ETL)=8} were obtained prior to intracardiac contrast administration and T1-weighted images were obtained immediately after contrast injection (0.2 mM/kg). Acquisition parameters included a field of view (FOV) of 4 cm, slice thickness of 0.5–1 mm, and a matrix size of 256×256 (in-plane resolution of 156×156 μm). Mice were anesthesized with isoflurane for these studies. Four mice from each category (Ras+Akt-induced GBMs, PDGF-induced low-grade oligodendrogliomas, high-grade PDGF-induced oligodendrogliomas) were studied.

Multiple Mouse Imaging

For screening larger numbers of mice, a parallel wound foil solenoid coil (Xu et al., submitted for publication) was used. In brief, the coil is a three-turn parallel wound foil solenoid (86 mm in diameter) designed for screening 13 to 15 mice simultaneously. This coil was interfaced directly to the Signa and required 20 dB of transmitter attenuation. Prior to study, a 24-gauge catheter was placed in the mouse tail vein. Subsequently, the mice were anesthesized and placed in the coil. Set-up time included approximately 5 to 10 min per mouse for tail vein catheterization and approximately 15 min for anesthesizing the mice subsequently and placing in the coil. The imaging protocol included sagittal scout

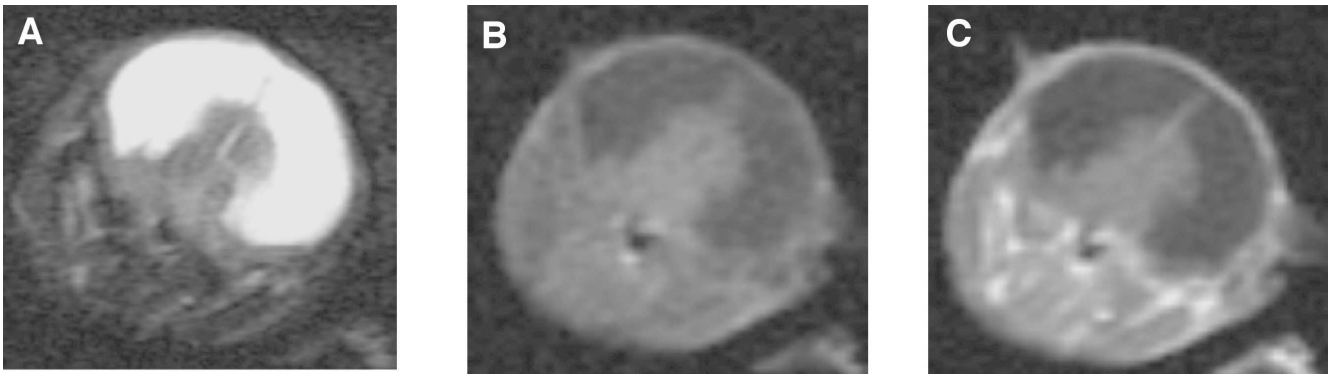

Figure 1. *T2- and T1-weighted (pre- and postcontrast) images from a mouse with hydrocephalus. The hyperintense signal in the T2-weighted images reflect the dilated lateral ventricles. Areas of hydrocephalus have high signal intensity on T2- and low signal intensity on T1-weighted image, reflecting the higher T1 and T2 values of fluid. Note the lack of enhancement postcontrast.*

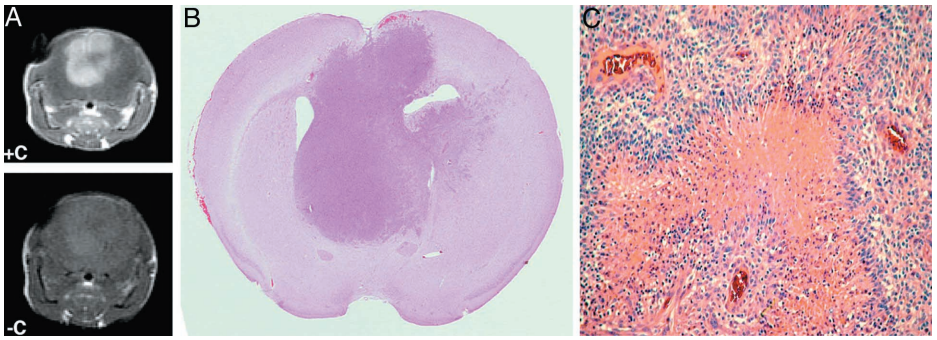

Figure 2. *Images and histopathologic sections of brain tumor obtained by infecting Ntv-a mice with combined RCAS-Ras and RCAS-Akt vectors. Images obtained with single mouse coil. (A) Intracranial tumor exhibits hyperintense signal on T2-weighted images and on postcontrast T1-weighted images. (B) Whole mount section corresponding to the images obtained by MRI. (C) Microscopic images of the GBM show histologic similarities to GBMs in humans.*

images followed by axial scout T2-weighted images, which each required less than 1 min. These were followed by high-resolution T2-weighted images, followed by a precontrast T1-weighted image. Subsequent to the contrast administration (0.2 mm/kg Gd-DTPA), T1-weighted images were obtained. The typical imaging parameters for T2-weighted images included a slice thickness of 1.5 mm and an in-plane resolution of 156×333 μm (FOV of 8 cm and an imaging matrix of 512×256), TR=4 to 6 s, TE=102 ms, an ETL of 16, and six excitations per phase-encoding step (imaging time of 6.4–9.6 min). On occasion, higher resolution scans (512×512) were obtained, which required longer acquisition times (up to 20 min). For T1-weighted images, the typical imaging parameters included a slice thickness of 1.5 mm and an in-plane resolution of 333×417 μm (FOV of 8 cm and an imaging matrix of 256×192), TR=300 ms, TE=9 ms, and three excitations per phase-encoding step (typical imaging time of approximately 2.9 min). Mice were anesthesized with ketamine (90 mg/kg) and xylazine (9 mg/kg) intraperitoneally for these studies. The total time in the magnet was about 35 to 40 min.

Results

Mice Developing Ras+Akt-Induced GBMs

Seventy percent of human GBMs show substantially elevated signaling through the Ras and Akt pathways [30]. These alterations appear to be responsible for the development of GBMs because activation of these pathways in mice results in the formation of gliomas with similarity to human GBMs. These mice were generated by intracranial injection of Ntv-a transgenic mice with the combination of DF-1 producer cells, generating RCAS-Ras and RCAS-Akt vectors. Approximately 20% to 30% of these transgenic mice develop gliomas. Mice with gliomas can be identified by the development of symptoms such as lethargy, hunched posture, weight loss, and poor grooming. However, these mice may also develop hydrocephalus that may or may not be associated with tumor development, and mice with hydrocephalus also develop similar symptoms. Figure 1 presents an image of a mouse with severe hydrocephalus. This is readily recognized as a bright area on T2-weighted images that does not enhance after Gd-DTPA.

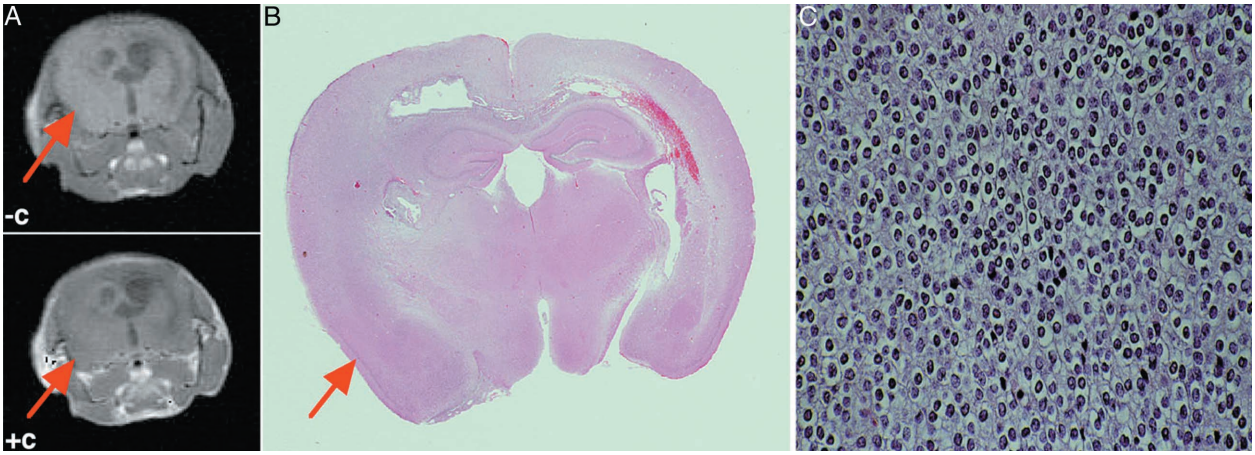

Figure 3. *Images and histopathologic sections of a brain tumor obtained by infecting Ntv-a mice with RCAS-PDGF. (A) Pre- and postcontrast MRI with lack of enhancement in the tumor region. (B) Corresponding whole mount brain section. (C) Microscopic histology of this tumor consistent with an oligodendroglioma.*

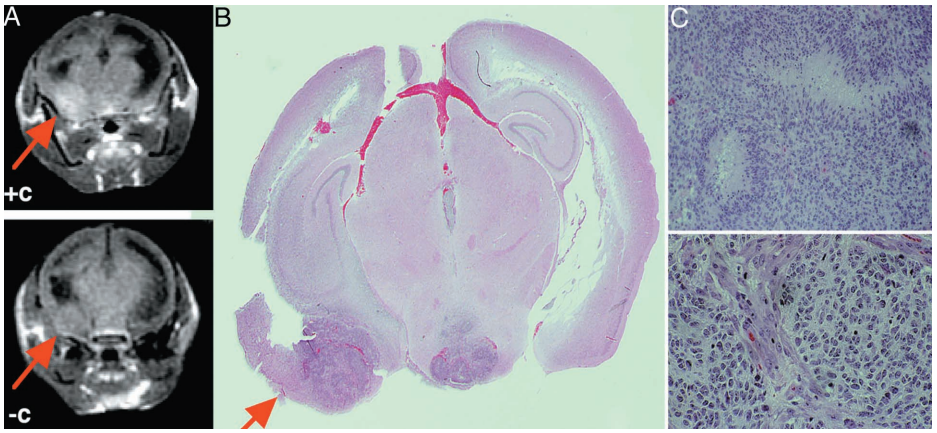

Figure 4. *Images and histopathologic sections of brain tumor obtained by infecting Ntv-a INK4a-ARF−/− mice with RCAS-PDGF. (A) Pre- and postcontrast MRI demonstrating lesion enhancement post Gd-DTPA (arrow). (B,C) Whole mount of the section shown in (A) revealing that the enhancing region has higher cellular density and necrosis.*

In order to determine if the imaging characteristics of GBMs developing in mice are similar to that seen in humans, Ntv-a mice were infected with combined RCAS-Ras and RCAS-Akt vectors. Several of these mice developed symptoms consistent with the presence of intracranial gliomas. These mice were anesthesized with isoflurane and imaged using the single mouse coil to demonstrate the presence of tumor. As illustrated in Figure 2*A*, intracranial tumors were readily identified by imaging on T1-weighted images post Gd-DTPA. These tumors enhanced with gadolinium contrast as seen in human GBMs, indicating disruption of the blood–brain barrier.

These mice were immediately sacrificed and the brains fixed in formalin. The brains were sectioned in the same plane to the MRI (Figure 2*B*). Pathological evaluation revealed nuclear pleomorphism, microvascular proliferation, pseudopalisading, and necrosis similar to the human GBM (Figure 2*C*).

PDGF-Induced Low-Grade Oligodendrogliomas

Ntv-a mice were infected with RCAS-PDGF as has been described [29]. These mice develop low-grade oligodendrogliomas. Mice developing intracranial symptoms were identified and scanned as described above using the single mouse coil (Figure 3*A*). These lesions do not enhance with intravenous contrast. As in the mice with GBMs, the mouse was sacrificed immediately after imaging and the brain was fixed and sectioned parallel to the plane of imaging (Figure 3*B*). Pathological evaluation revealed an oligodendroglioma including regular round nuclei, cleared cytoplasm, and lack of immunohistochemical staining of tumor cells with antibodies to the astrocytic marker glial fibrillary acetic protein.

High-Grade PDGF-Induced Oligodendrogliomas

High-grade gliomas in humans frequently have deletions in the INK4a-ARF tumor suppressor gene and therefore do not express either $p16^{INK4a}$ or $p14^{ARF}$ tumor suppressor gene products that control cell cycle arrest. PDGF-induced gliomas in mice with a targeted deletion of INK4a-ARF have the propensity to show high-grade characteristics such as microvascular proliferation, and pseudopalisading necrosis has been previously demonstrated. Therefore, Ntv-a INK4a-ARF−/− mice were infected with RCAS-PDGF. Mice developing symptoms were identified and scanned as above, with findings illustrated in Figure 4. A portion of the lesion enhanced after administration of intravenous contrast. Comparison with the whole mount demonstrates that these enhancing regions correspond to areas of higher cellular density and necrosis. Histological analysis of the vasculature of the enhancing and nonenhancing regions of the tumors showed other parallels with the human disease. The

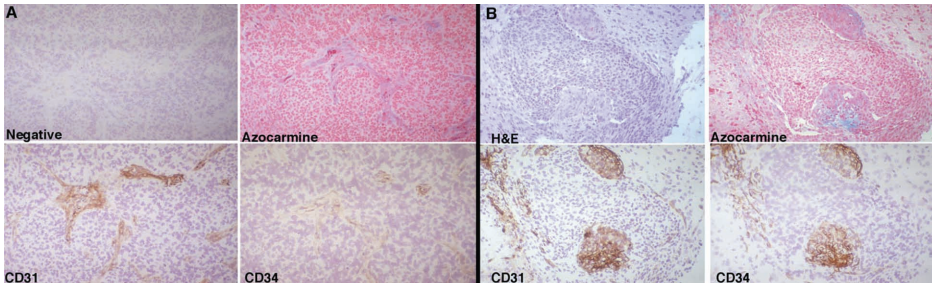

Figure 5. *Histologic analysis of the vasculature of the enhancing and nonenhancing regions of the tumor from Figure 4. (A) Nonenhancing regions of tumor have "chicken wire" vasculature (arrow) seen in human low-grade oligodendrogliomas. (B) Regions of tumor that enhanced with gadolinium showed glomeruloid microvascular proliferation similar to that seen in high grade oligodendrogliomas.*

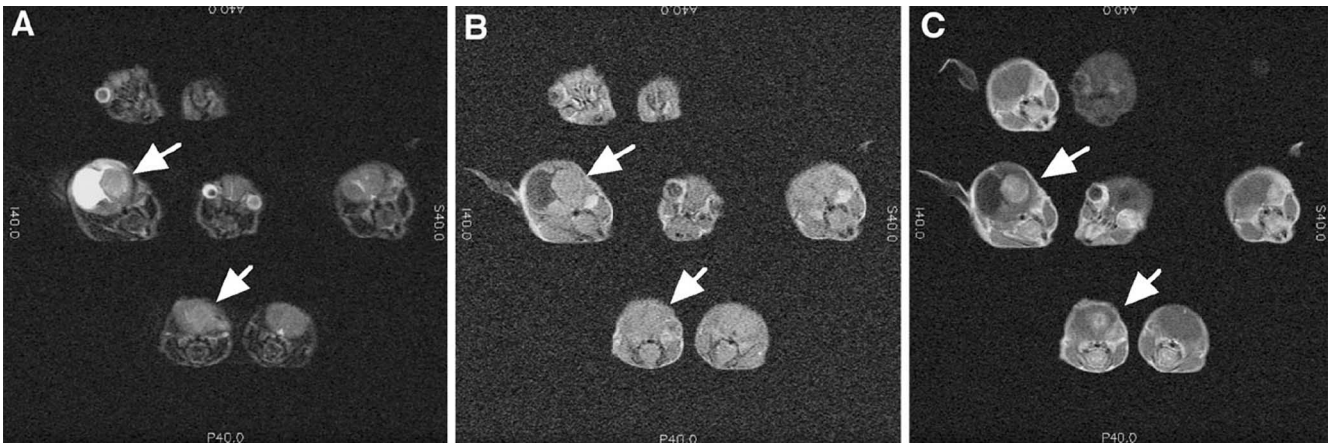

Figure 6. *Images obtained on Ntv-a mice that had been infected with the combination of RCAS-Akt and RCAS-Ras. Plates (A), (B), and (C) are T2. T1 (precontrast) and T1 (postcontrast) from a single slice of multiple mice. Arrows indicate tumor as seen best on post Gd-DTPA images. Areas of hyperintense signal in the T2-weighted images correspond to areas of hydrocephalus, which are noted to not enhance with Gd-DTPA. Acquisition parameters included TR = 5500 ms, TE = 102 ms, NEX = 4, 512×512, 8×8 cm^2, slice thickness = 1.5 mm, gap = 0.5 mm.*

nonenhancing regions of tumor demonstrated the chicken wire vasculature seen in human low-grade oligodendrogliomas (Figure 5*A*). By contrast, the regions of tumor that enhanced with gadolinium showed glomeruloid microvascular proliferation similar to that seen in high-grade gliomas (Figure 5*B*). Therefore, the regions of enhancement within this diffuse tumor correlate with high-grade histology and similar vascular abnormalities as seen in the human disease.

Obtaining Images on Multiple Mice with Possible Gliomas Simultaneously

In order to determine if the multimouse imaging coil would be able to identify mice harboring gliomas within a population of mice, Ntv-a mice that had been infected with the combination of RCAS-Akt and RCAS-Ras were screened. Mice that had developed symptoms described above were anesthesized and imaged. Figure 6*A* shows a T2-weighted scan, which shows seven mice in the plane of the image. Two of these mice had findings suggestive of a brain tumor. In addition to being detected on the T2-weighted image, the tumors are readily distinguished from the high signal intensity areas seen with hydrocephalus. The T1-weighted pre- and postcontrast images, respectively, reveal, as in the clinical situation, contrast enhancement after Gd-DTPA injection (0.2 mm/kg) on T1-weighted images. These images demonstrate the feasibility of successfully screening mice quickly using medium resolution images and very sensitive solenoid coils to detect mice that develop brain tumors.

To evaluate the contrast between normal brain and tumor, the ratio of signal intensity of tumor *versus* brain was measured. The T2-weighted images had a tumor/brain signal intensity ratio of 1.003±0.06 (mean±SEM). For T1-weighted images precontrast administration, the ratio was 1.13±0.10. For T1-weighted images postcontrast, the ratio was 13.35±1.51, which was highly significant ($P<.001$). Low-grade gliomas failed to enhance, indicating that MRI can distinguish high-grade gliomas and distinguish between high- and low-grade gliomas.

Discussion

Animal modeling of cancer formation allows not only the identification of causative factors in tumor formation but also provides tumor-bearing animals for the testing of experimental therapeutics [31]. The use of mice with tumors identified by imaging techniques in preclinical trials allows each mouse to be used as its own control and substantially expands the information that can be obtained from such trails. In the absence of imaging data, population studies requiring large numbers of mice need to be undertaken. If one estimates that 20% of the mice have tumors and a cohort size of 6 to 10 tumor-bearing mice is necessary for evaluating a treatment, one can reduce the size of each cohort from 30–50 to 6–10 mice by using imaging to identify appropriate mice.

Many new imaging techniques that help distinguish various characteristics of tumors are being developed. However, in humans, the pathological correlation among the image, the genetics, and the histology is often not possible. The combination of imaging techniques and animal models for gliomas will allow such correlations and not only validate the models as similar to the human disease, but also validate the imaging techniques as representing the pathology proposed.

The development of novel transgenic and knockout mice, which do not predictably develop tumors with 100% penetrance, emphasizes the need for a screening technique. MRI, either at high spatial resolution or even at moderate resolution such as obtained with the coil used for multiple mouse imaging, has the potential to address this need using moderate spatial resolution scans as demonstrated. Despite the loss of some spatial resolution compared to other techniques, detection of these tumors is quite easy because they are visualized on T2-weighted images and also on T1-weighted (postcontrast) studies. The amount of magnet time necessary for studying 13 mice is about 40 min. Conceivably, one could forego the T2-weighted images (~6–10 min) because the postcontrast T1-weighed images are "diag-

nostic'' and would allow one to screen up to about 26 mice in an hour. We estimate that we can screen about 150 mice per day based on these imaging times, which should be adequate to meet the needs of most experimental research groups. It is likely that this will represent an upper limit or even slight overestimate because it is expected that some mice might be restudied at higher spatial resolution if there are areas that are suspicious for small tumors. The times required for catheter placement, anesthesia, and placing the mice in the coil are not significant because the limiting resource is magnet time and these activities occur while other mice are undergoing study. We have been able to detect tumors as small as 0.8 mm in axial diameter, although with tumors less than 1 mm diameter, some lesions were missed (three of eight tumors smaller than 1 mm were detected). All tumors greater than 1.5 mm in diameter ($n=9$) were detected.

These imaging systems are currently in use in preclinical trials of small molecule inhibitors of signal transduction pathways. These systems provide the ability to look at immediate responses at the imaging, histologic, and genetic levels to disruption of the pathways that induce gliomas.

Acknowledgements

We thank Joseph Celestino for his help in imaging the mice and histologic analysis at MD Anderson; Eddie Nerio for histologic analysis at MSKCC; and Eddy Boskamp of General Electric Medical Systems for designing and constructing the mouse coil. The authors are grateful for support from the NIH (R24CA83084-1, UO1 CA894314-1, CA-08748) and the Searle, Tow, and Bressler Scholar's programs.

References

[1] Graif M, Bydder GM, Steiner RE, Niendorf P, Thomas DG, and Young IR (1985). Contrast-enhanced MR imaging of malignant brain tumors. *Am J Neuroradiol* **6**, 855–62.

[2] Roberts HC, Roberts TP, Brasch RC, and Dillon WP (2000). Quantitative measurement of microvascular permeability in human brain tumors achieved using dynamic contrast-enhanced MR imaging: correlation with histologic grade. *Am J Neuroradiol* **21**, 891–99.

[3] Provenzale JM, Wang GR, Brenner T, Petrella JR, and Sorenson AG (2002). Comparison of permeability in high-grade and low-grade brain tumors using dynamic susceptibility contrast MR imaging. *Am J Roentgenol* **178**, 711–16.

[4] Blankenberg F, Conley FK, Sayre J, and Enzmann D (1991). MR imaging in an experimental model of brain tumor immunotherapy. *Am J Neuroradiol* **12**, 543–48.

[5] Chenevert TL, McKeever PE, and Ross BD (1997). Monitoring early response of experimental brain tumors to therapy using diffusion magnetic resonance imaging (1997). *Clin Cancer Res* **3**, 1457–66.

[6] Kim B, Chenevert TL, and Ross BD (1995). Growth kinetics and treatment response of the intracerebral rat 9 L brain tumor model: a quantitative *in vivo* study using magnetic resonance imaging. *Clin Cancer Res* **1**, 643–50.

[7] Kish PE, Blaivas M, Strawderman M, Muraszko KM, Ross DA, Ross BD, and McMahon G (2001). Magnetic resonance imaging of ethylnitrosourea–induced rat gliomas: a model for experimental therapeutics of low-grade gliomas. *J Neuro-Oncol* **53**, 243–57.

[8] Sherburn EW, Wanebo JE, Kim P, Song SK, Chicoine MR, and Woolsey TA (1999). Gliomas in rodent whisker barrel cortex: a new tumor model. *J Neurosurg* **91**, 814–21.

[9] Chenevert TL, Stegman LD, Taylor JM, Robertson PL, Greenberg HS, Rehemtulla A, and Ross BD (2000). Diffusion magnetic resonance imaging: an early surrogate marker of therapeutic efficacy in brain tumors. *J Natl Cancer Inst* **92**, 2029–36.

[10] Stegman LD, Rehemtulla A, Hamstra DA, Rice DJ, Jonas SJ, Stout KL, Chenevert TL, and Ross BD (2000). Diffusion MRI detects early events in the response of a glioma model to the yeast cytosine deaminase gene therapy strategy. *Gene Ther* **7**, 1005–10.

[11] Evelhoch JL, Gillies RJ, Karczmar GS, Koutcher JA, Maxwell RJ, Nalcioglu O, Raghunand N, Ronen SM, Ross BD, and Swartz HM (2000). Applications of magnetic resonance in model systems: cancer therapeutics. *Neoplasia* **2**, 152–65.

[12] Kaplan O, Firon M, Vivi A, Navon G, and Tsarfaty I (2000). HGF/SF activates glycolysis and oxidative phosphorylation in DA3 murine mammary cancer cells. *Neoplasia* **2**, 365–77.

[13] Fleige G, Nolte C, Synowitz M, Seeberger F, Kettenmann H, and Zimmer C (2001). Magnetic labeling of activated microglia in experimental gliomas. *Neoplasia* **3**, 489–99.

[14] Bhujwalla ZM, Artemov D, Natarajan K, Ackerstaff E, and Solaiyappan M (2001). Vascular differences detected by MRI for metastatic *versus* nonmetastatic breast and prostate cancer xenografts. *Neoplasia* **3**, 143–53.

[15] Pilatus U, Ackerstaff E, Artemov D, Mori N, Gillies RJ, and Bhujwalla ZM (2000). Imaging prostate cancer invasion with multi-nuclear magnetic resonance methods: the Metabolic Boyden Chamber. *Neoplasia* **2**, 273–79.

[16] Fujimoto JG, Pitris C, Boppart SA, and Brezinski ME (2000). Optical coherence tomography: an emerging technology for biomedical imaging and optical biopsy. *Neoplasia* **2**, 9–25.

[17] Vajkoczy P, Ullrich A, and Menger MD (2000). Intravital fluorescence videomicroscopy to study tumor angiogenesis and microcirculation. *Neoplasia* **2**, 53–61.

[18] Ramanujam N (2000). Fluorescence spectroscopy of neoplastic and non-neoplastic tissues. *Neoplasia* **2**, 89–117.

[19] Edinger M, Sweeney TJ, Tucker AA, Olomu AB, Negrin RS, and Contag CH (1999). Noninvasive assessment of tumor cell proliferation in animal models. *Neoplasia* **1**, 303–10.

[20] Contag CH, Jenkins D, Contag PR, and Negrin RS (2000). Use of reporter genes for optical measurements of neoplastic disease *in vivo*. *Neoplasia* **2**, 41–52.

[21] Paulus MJ, Gleason SS, Kennel SJ, Hunsicker PR, and Johnson DK (2000). High resolution X-ray computed tomography: an emerging tool for small animal cancer research. *Neoplasia* **2**, 62–70.

[22] Ponomarev V, Doubrovin M, Lyddane C, Beresten T, Balatoni J, Bornman W, Finn R, Akhurst T, Larson S, Blasberg R, Sadelain M, and Tjuvajev JG (2001). Imaging TCR-dependent NFAT-mediated T-cell activation with positron emission tomography *in vivo*. *Neoplasia* **3**, 480–88.

[23] Gambhir SS, Herschman HR, Cherry SR, Barrio JR, Satyamurthy N, Toyokuni T, Phelps ME, Larson SM, Balatoni J, Finn R, Sadelain M, Tjuvajev J, and Blasberg R (2000). Imaging transgene expression with radionuclide imaging technologies. *Neoplasia* **2**, 118–38.

[24] Gambhir SS, Barrio JR, Phelps ME, Iyer M, Namavari M, Satyamurthy N, Wu L, Green LA, Bauer E, MacLaren DC, Nguyen K, Berk AJ, Cherry SR, and Herschman HR (1999). Imaging adenoviral-directed reporter gene expression in living animals with positron emission tomography. *Proc Natl Acad Sci USA* **96**, 2333–38.

[25] Mankoff DA, Dehdashti F, and Shields AF (2000). Characterizing tumors using metabolic imaging: PET imaging of cellular proliferation and steroid receptors. *Neoplasia* **2**, 71–88.

[26] Fisher GH, Orsulic S, Holland EC, Hively WP, Li Y, Lewis BC, Williams BO, and Varmus HE (1999). Development of a flexible and specific gene delivery system for production of murine tumor models. *Oncogene* **38**, 5253–60.

[27] Holland EC, Hively W, DePinho R, and Varmus H (1998). A constitutively active epidermal growth factor receptor cooperates with disruption of G1 cell-cycle arrest pathways to induce glioma-like lesions in mice. *Genes Dev* **12**, 3675–85.

[28] Holland EC, and Varmus H (1998). Basic fibroblast growth factor induces cell migration and proliferation after glia-specific gene transfer in mice. *Proc Natl Acad Sci USA* **95**, 1218–23.

[29] Dai C, Celestino J, Okada Y, Louis DN, Fuller GN, and Holland EC (2001). PDGF autocrine stimulation dedifferentiates cultured astrocytes and induces oligodendrogliomas and oligoastrocytomas from neural progenitors and astrocytes *in vivo*. *Genes Dev* **15**, 1913–25.

[30] Holland EC, Celestino J, Dai C, Schaefer L, Sawaya RE, and Fuller GN (2000). Combined activation of Ras and Akt in neural progenitors induces glioblastoma formation in mice. *Nat Genet* **25**, 55–57.

[31] Holland EC (2001). Gliomagenesis: genetic alterations and mouse models. *Nat Rev Genet* **2**, 120–29.